



Development, dielectric response and functionality of SrTiO₃/epoxy nanocomposites

G. C. Manika¹ · G. C. Psarras¹

Received: 19 March 2019 / Accepted: 25 June 2019 / Published online: 3 July 2019
© Springer Science+Business Media, LLC, part of Springer Nature 2019

Abstract

Composite systems of epoxy resin and SrTiO₃ nanoparticles have been prepared and studied in different filler concentrations. Scanning electron microscopy (SEM) and X-ray diffraction (XRD) revealed that there was a successful filler integration and fine dispersion in the polymer matrix. Moreover, Broadband dielectric spectroscopy (BDS) was employed for the determination of the dielectric response of all manufactured systems. Dielectric results divulge three relaxation processes which are referred to: (a) glass to rubber transition of the polymer matrix (α -mode), (b) re-arrangement of polar side groups of the polymer matrix (β -mode) and (c) interfacial polarization between systems' components. It was found that all nanodielectric systems exhibit enhanced dielectric properties which are mainly attributed to the semiconductive nanoinclusions and to the extended interface between the polymer matrix and the nanofiller. Finally, dynamic analysis of the relaxation processes was also performed. Vogel–Fulcher–Tammann equation describes the α -mode's loss peak dependence on temperature, whereas the β -mode follows the Arrhenius expression. In case of β -mode it was found that the presence of the nanoinclusions hinders the orientation of the matrix's polar side groups.

1 Introduction

The integration of inorganic nanoparticles in polymer matrix allows the coupling of both matrix's and nanofiller's properties into the polymer composite, achieving increased functionality. Therefore, nanocomposite materials have emerged as suitable alternatives for overcoming the limitations of microcomposites and monolithics and can be considered as a novel class of engineering materials with enhanced applicability. More specifically, this kind of materials can be employed in technological applications such as: hybrid electric vehicles, cellular phones, microelectronic devices etc. Nanocomposites are defined as multiphase solid materials with at least one of the components to have nanoscaled structure. Nanodielectrics refer to dielectric materials which comprise entities with dimensions at the nanometric scale. These materials have attracted a lot of scientific interest due to their novel physical properties (optical, electrical, magnetic), depending on their morphology and interfacial

characteristics of the components. While the particle size of the reinforcing phase decreases, the ratio of surface/volume increases, so the surface properties become crucial, achieving enhanced thermomechanical, rheological, electrical and optical properties. The electrical performance arises from the combination of the high breakdown strength of the polymer matrix, the high permittivity values of nanofiller and the interfacial phenomena. The type and the amount of the nanoinclusions tailor the dielectric behaviour of nanodielectric composites [1–10]. Nanocomposite materials consisted of an amorphous polymer matrix and ceramic nanofiller are considered as heterogeneous disorder systems in which their electrical properties are directly related to the electric permittivity and conductivity of their constituents, the volume fraction of the filler and the size and shape of the particles.

Ceramic strontium titanate (SrTiO₃) nanoparticles and an epoxy resin were employed as the reinforcing phase and polymer matrix respectively. Epoxy resin exhibits a lot of advantages, such as, resistance to corrosive environments, good thermomechanical behaviour, ease in molding etc. and for these reasons it was preferred as the polymer matrix. On the other hand, SrTiO₃ is a complex oxide having a simple perovskite structure (ABO₃). SrTiO₃ has high charge storage capacity so it has potential applicability in electronic devices as a high dielectric constant material. In recent years SrTiO₃

✉ G. C. Psarras
G.C.Psarras@upatras.gr

¹ Smart Materials & Nanodielectrics Laboratory, Department of Materials Science, University of Patras, 26504 Patras, Greece

has been used widely as a substrate for epitaxial growth of high temperature semiconducting films as a wide band gap semiconductor with a band gap of 3.2 eV. In addition, SrTiO₃ has a simple cubic lattice Pm3 m, which at the critical temperature ($T_C = 105$ K) undergoes, upon cooling, a ferroelectric transition from the cubic to the tetragonal structure [11–13]. Moreover, SrTiO₃ is often termed as an incipient ferroelectric, since its dielectric behaviour, at low temperatures, is mainly attributed to the quantum fluctuations and preceding antiferrodistortive structural phase transition. In the case of a quantum paraelectric the dielectric constant diverges until reaching a temperature low enough, ~ 4 K in the case of SrTiO₃, where quantum effects are able to cancel ferroelectricity [11, 12]. These unique properties make SrTiO₃ a very attractive reinforcing phase candidate for the development of nanocomposites and consequently there is interest in studying their dielectric properties.

In this work nanocomposites constituted of an epoxy resin (ER) as a matrix and strontium titanate (SrTiO₃) nanoparticles as the reinforcing phase, have been prepared and studied at various filler contents. The prepared nanocomposites were first morphologically characterized via X-ray diffraction (XRD) and Scanning electron microscopy (SEM). Their dielectric properties and the relaxation phenomena were studied by means of Broadband dielectric spectroscopy (BDS) in the temperature and frequency range of 30–160 °C and 0.1 Hz to 10 MHz respectively. Dielectric analysis reveals relaxations processes related to both polymer matrix and ceramic nanofiller. Finally, relaxation dynamics analysis was performed in the recorded relaxation processes.

2 Experimental details

2.1 Sample preparation

The preparation of the nanocomposites was performed by employing commercially available materials. The polymer matrix phase was developed by combining a low viscosity epoxy resin (ER) (bisphenol-A) with a slow rate reacting cycloaliphatic amine as curing agent. Both reactants, with trade names Epoxol 2004A and Epoxol 2004B respectively, were provided by Neotex S.A. Strontium titanate (SrTiO₃) nanoparticles were purchased from Sigma Aldrich and as it is stated in their datasheet, their diameter is less than 100 nm. The fabrication procedure consisted of the following steps: (i) the epoxy resin (ER) matrix was prepared by mixing in 2:1 (w/w) ratio of the epoxy prepolymer and the curing agent. (ii) As the polymer matrix was in the liquid state pre-calculated amounts of SrTiO₃ nanofiller were added. (iii) The resulting mixtures were subsequently stirred at a slow rate under ultrasonication avoiding thus the creation of clusters. (iv) The homogenized mixtures were poured

to moulds and (v) the initial curing process took place at ambient conditions for a week, followed by post-curing at 100 °C for 4 h. The curing and post-curing procedures have been established via several test methods. The selection of a high post-curing temperature targets to the mechanical stability of the polymer via the completion of the cross-linking process.

The SrTiO₃ content of the prepared nanocomposites was expressed in parts per hundred resin (phr) per mass and were: 0 (unreinforced epoxy), 3, 7, 10, 12 and 15 phr.

2.2 Methods

2.2.1 X-ray diffraction (XRD)

A Bruker AXS D8 Advance device with a Bragg-Bretano geometry was employed for the conduction of XRD analysis. More specifically, a LynxEye detector and Cu K α spectral line (line ($\lambda = 1.54062$ Å) was used as the incident radiation. The slit of the source was 0.6 mm and the current and voltage source were set at 40 kV and 40 mA, respectively. Finally, the scan mode was continuous with an angle step of 0.02° (2 θ) and the scan speed was 0.5 s/step.

2.2.2 Scanning electron microscopy (SEM)

Nanocomposite's morphology, the quality of nanofiller dispersion, along with the existence of agglomerates, voids and clusters inside the polymer matrix were investigated by means of SEM (Carl Zeiss EVO MA 10).

2.2.3 Differential scanning calorimetry (DSC)

DSC measurements were conducted by a TA Q200 device (TA Instruments). The scan rate operation was 5 °C/min and the samples were placed in an aluminum crucible, while an empty one was used as reference. The temperature range was from 30 to 160 °C.

2.2.4 Broadband dielectric spectroscopy (BDS)

All nanocomposites were electrically characterized by means of BDS. The frequency range was varied from 0.1 Hz to 10 MHz via an Alpha-N Frequency Response Analyzer, which was supplied by Novocontrol Technologies. The temperature was tailored by Novotherm system (Novocontrol Technologies) with ± 0.1 °C accuracy, while the applied V_{rms} was constant at 1 V. A two gold-plated dielectric system (BDS 1200) was used as the dielectric cell. Isothermal frequency scans were performed for every nanocomposite system from ambient to 160 °C with a temperature step of 5 °C. The real time acquisition of all data was conducted via

Windeta software. Dielectric measurements were conducted according to the ASTM D150 specifications.

3 Results and discussion

3.1 Structural and morphological characterization of SrTiO₃ nanocomposites

After the preparation of SrTiO₃/epoxy samples, XRD patterns were recorded in order to confirm the successful fabrication of nanocomposites. Specimens' morphology was also examined via SEM. Figure 1a depicts the XRD patterns of all examined systems. It is evident that there is successful integration of the filler in the polymer matrix. Scherrer formula was employed for the determination of the SrTiO₃ nanoparticle's size, Eq. (1).

$$D(\text{nm}) = \frac{K \cdot \lambda}{\beta \cdot \cos \theta} \quad (1)$$

where $K = 0.9$, $\lambda = 1.54062 \text{ \AA}$ which is the wavelength of X-ray, β is Full width at half maximum (FWHM) of each peak and θ is the Bragg angle. It was found that the average size of nanofillers is 28.0 nm.

Epoxy resin, as an amorphous component, has no diffraction peaks, so the recorded peaks of the composite systems correspond to the SrTiO₃ nanoinclusions. Moreover, peaks' intensity increases with filler content, while the spectrum of SrTiO₃ nanoparticles is also presented as a reference. Figure 1b presents an indicative SEM image of cryo-fractured surface for the 15 phr SrTiO₃ nanocomposite. The dispersion of nanofillers in the polymer matrix can be considered fine and homogeneous without extensive aggregates, even at the highest content of nanoinclusions. The size dispersion of nanoparticles has been determined by employing Image J software and interpreting SEM image (15 phr SrTiO₃). It was found that there is a wide dispersion of sizes, with two major counterparts ranging between 40–60 and 80–100 nm (Fig. 1c).

3.2 Dielectric characterization of SrTiO₃ nanocomposites

Polymer matrix nanocomposites are mainly electrical insulators due to the fact that the concentration of free charge carriers is very low. Thus, their electrical properties are associated to the dielectric relaxation phenomena occurring under the influence of AC field. These relaxation processes basically concern the dipolar orientation effects of both permanent and induced dipoles and in some cases to the space charge migration. The presence of nanofiller affects these relaxations processes in multiple ways. Therefore, it is crucial to examine the influence of nanoinclusions upon these

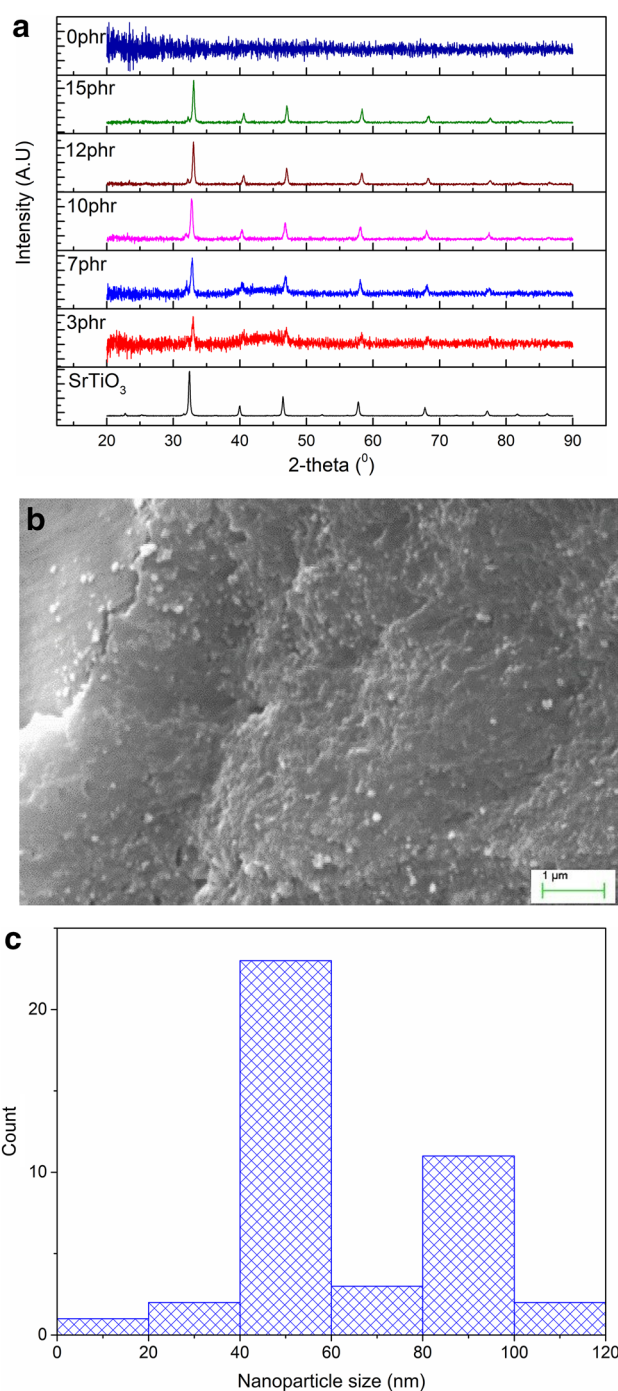


Fig. 1 a XRD patterns of SrTiO₃ nanoparticles and all studied nanocomposites, b SEM image of the 15 phr SrTiO₃/epoxy nanocomposite and c dispersion of nanoparticles' size in the 15 phr SrTiO₃ nanocomposite as determined via Image J software

relaxation processes. Dielectric spectra of such systems appear to be complex. The SrTiO₃ nanocomposite systems were electrically characterized via BDS. 3D dielectric spectra of the real part of dielectric permittivity, loss tangent and conductivity as a function of temperature and frequency, are

represented for the 7 phr SrTiO₃ reinforced nanocomposite in Fig. 2a, b and c respectively.

As a wide band gap semiconductor, SrTiO₃ exhibits higher values of ϵ' than the corresponding ones of the insulating matrix. Thus, the nanoreinforced SrTiO₃ systems acquire higher values of ϵ' in comparison with the epoxy resin in the whole frequency and temperature ranges. Figure 2a indicates the dependence of the real part of permittivity upon the frequency of the applied electrical field, ϵ' diminishes with the increase of frequency. At lower frequencies dipoles attain sufficient time to orient themselves in the direction of the altering field and for this reason ϵ' gets higher values. By the same token, as the frequency increases dipoles fail to be aligned in the direction of the AC field, resulting in low polarization level and ϵ' values. Furthermore, temperature facilitates the polarization process due to the thermal agitation of the dipoles, as a result ϵ' acquires high values in the range of low frequencies and high temperatures. 3D permittivity spectra (Fig. 2a) show two step-like

transitions, implying the presence of dielectric relaxation processes. These relaxation processes are more evident in the 3D loss tangent spectra (Fig. 2b). Figure 2b shows the formation of three peaks, indicating the presence of three relaxation processes. More specifically, at intermediate frequencies and temperatures, a strong relaxation process appears which is related to the glass to rubber transition of the amorphous polymer matrix (α -relaxation). At the low frequency and high temperature range a second relaxation process is observed, which is attributed to interfacial polarization (IP) process. Interfacial polarization process mainly appears in electrically heterogeneous systems of two or more phases and it is also known as Maxwell-Wagner Sillars (MWS) effect. At the constituents' interface large dipoles are formed, because of the accumulation of unbounded charges, exhibiting time delay in their orientation parallel to the field as the applied field's frequency increases, leading to IP vanish. The third relaxation process is observed at high frequencies, and is associated with the re-orientation of the

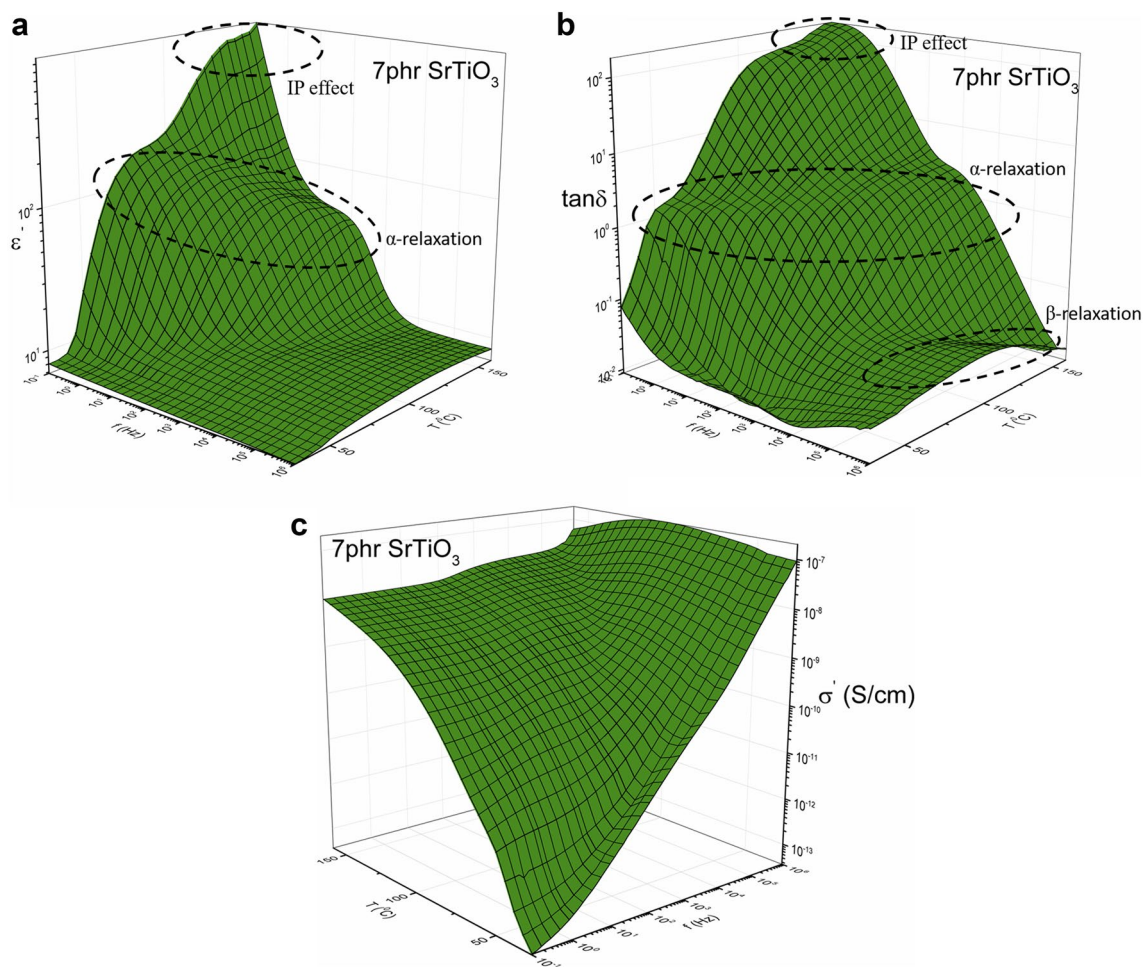


Fig. 2 Dielectric spectra of the 7 phr SrTiO₃ nanocomposite as a function of temperature and frequency for the: **a** real part of dielectric permittivity, **b** loss tangent and **c** AC conductivity

polar side groups of the main polymer chain (β -relaxation). Figure 2c exhibits the variation of σ_{AC} with temperature and frequency. It is evident that at low frequencies the influence of the temperature is more pronounced, revealing a thermally activated conduction mechanism. The temperature impact decreases with frequency, and in the high frequency range σ_{AC} appears to be temperature independent. At constant temperature σ_{AC} follows Eq. (2):

$$\sigma_{AC}(\omega) = \sigma_{DC} + A(\omega)^s \quad (2)$$

where σ_{DC} is the $\omega \rightarrow 0$ limiting value of $\sigma_{AC}(\omega)$ and A, s are parameters depending on temperature and filler content. Equation (2) is often called the “The AC universality law” due to its general validity [14–16].

In the low frequency range, charge carriers are forced to migrate over larger distances and their transport is confined by the presence of isolated conductive sites within the insulating matrix. At high frequencies localized charge carriers motion takes maximum advantage of adjacent conductive regions by executing jumps (hops) between of them. Figure 2c indicates that as the temperature increases the exponential part of the σ_{AC} curves shifts to higher frequencies. Finally, at intermediate frequencies the presence of “shoulder-like” peaks is evident, which are related to the dielectric relaxations phenomena occurring in this frequency range. Figure 3a depicts comparative plots of ϵ' as a function of frequency at 30 °C, while Fig. 3b presents the variation of ϵ' as a function of temperature at 0.1 Hz, for all studied systems.

Figure 3a shows that all reinforced systems exhibit higher ϵ' values in comparison with the epoxy resin. The specimen with the highest filler loading does not exhibit the maximum ϵ' value, indicating that the optimum performance does not correspond to the maximum filler content. This deviation probably expresses the existence of particle clusters in the nanocomposite with the maximum filler loading. Figure 3b indicates that at low temperatures and frequencies,

temperature seems to have negligible or limited impact on ϵ' , which acquires low values. α -relaxation is evident in the temperature range between 50 and 80 °C, where ϵ' values increase due to the enhanced mobility of large segments of the main polymer chain. At high temperatures ϵ' of all specimens gradually increases due to the IP effect. Figure 4 depicts the variation of loss tangent with frequency at 160 °C for all SrTiO₃/epoxy nanocomposites. In these spectra all three relaxation processes are recorded. α -relaxation appears at intermediate frequencies, while at high frequencies the β -relaxation is also evident. Finally, at low frequencies (see also inset in Fig. 4) IP is present.

In addition, glass transition temperature was also determined by differential scanning calorimetry (DSC) tests. Figure 5 depicts the obtained DSC thermographs, along with the corresponding T_g values. Glass transition temperatures were

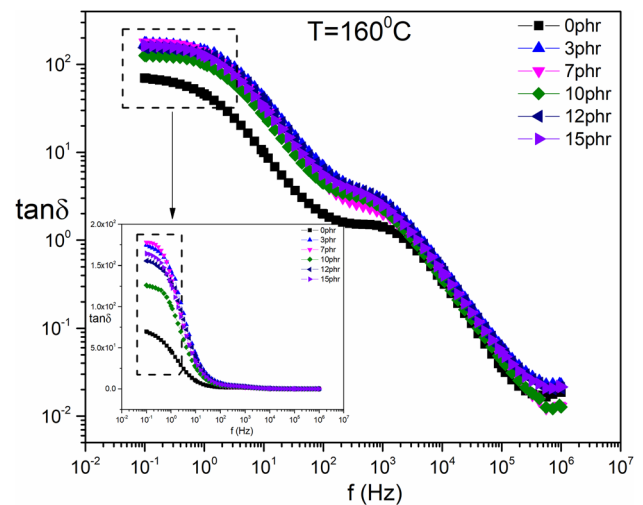


Fig. 4 Loss tangent ($\tan \delta$) as a function of frequency at 160 °C for all SrTiO₃ nanocomposites

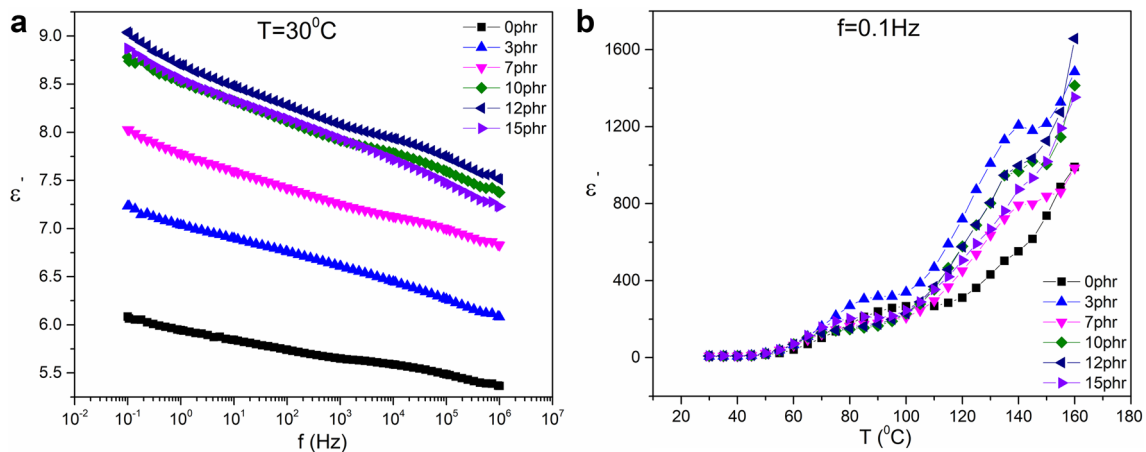


Fig. 3 ϵ' of all nanocomposite systems **a** as a function of frequency at 30 °C and **b** as a function of temperature at 0.1 Hz

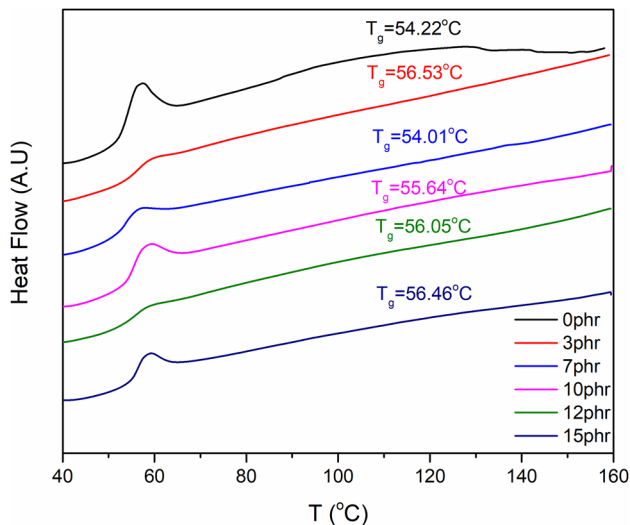


Fig. 5 DSC thermographs of all specimens with a heating rate of 5 °C/min and the variation of T_g values

determined by employing suitable software and the point of inflection of the curves at the recorded transitions. It is evident that there is a tendency for an increment of T_g values as the reinforcing phase increases. This finding implies that there are attractive interactions at the interface between the polymer matrix and the nanofiller. In polymer nanocomposites, glass to rubber transition is not only related to the chemical structure of the polymer but also to the type of the reinforcing phase. As it has been already cited, variation of glass transition temperature as a function of nanofiller can be also described via BDS. In the vicinity of T_g temperature, macromolecules acquire sufficient mobility in order to relax synergistically under the influence of the AC electric field. This relaxation gives rise to the formation of a loss peak, which is evident in both permittivity and $\tan\delta$ spectra (Fig. 2a, b).

Nanocomposites exhibit functional behaviour which is mainly attributed to the variation of different physical properties, such as polarization or conductivity upon temperature and frequency. In this work, the amplitude of the applied field was constant, and the samples' thickness had small variations, resulting in a modification of the exerted field from sample to sample. Therefore, in order to remove the influence of geometry upon the produced polarization and to find a way to relate the functional behaviour with materials' properties Dielectric reinforcing function (DRF) was employed. DRF is defined by Eq. (3) [17, 18]:

$$G(\omega, T) = \frac{\epsilon'_{comp}(\omega, T)}{\epsilon'_{mat}(\omega, T)} \quad (3)$$

where $\epsilon'_{comp}(\omega, T)$ and $\epsilon'_{mat}(\omega, T)$ is the real part of dielectric permittivity of the composite and the matrix respectively,

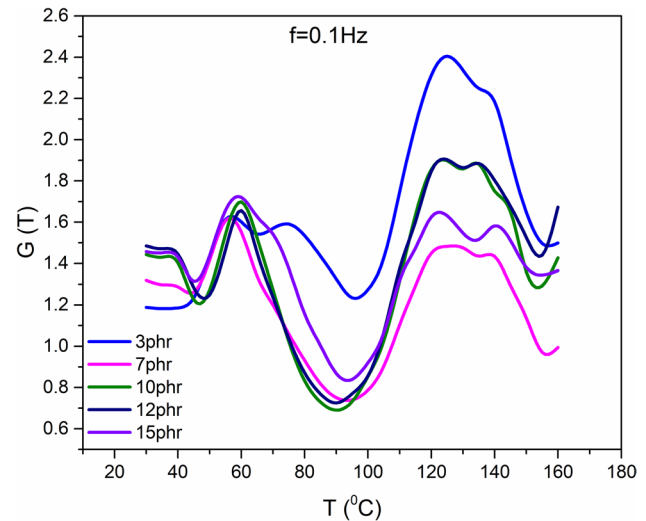


Fig. 6 DRF as a function of temperature at 0.1 Hz for all SrTiO₃/epoxy nanocomposites

while ω is the angular frequency and T the temperature of the sample. In case of isochronal conditions Eq. (3) transforms to Eq. (4):

$$G(T) = \frac{\epsilon'_{comp}(T)}{\epsilon'_{mat}(T)} \quad (4)$$

DRF can be considered as a normalized measure of polarization, reflecting the dielectric contribution of the reinforcing filler and the efficiency of energy storage. Figure 6 depicts the variation of DRF upon temperature under isochronal conditions (0.1 Hz). It is apparent the formation of two sets of peaks in all SrTiO₃ nanocomposites. In the temperature range of 50–70 °C α -relaxation process appears, which is associated with the glass to rubber transition of the polymer matrix. The second set of peaks recorded between 120 and 140 °C is associated with the IP effect. The formation of double-like peaks in this region, related to interfacial polarization process, is attributed to the nanoparticles' size dispersion. As indicated by Fig. 1c, the average size for the majority of nano-inclusions lies within the ranges 40–60 and 80–100 nm. The size of the formed dipoles at the interfaces varies with nano-inclusions' dimensions. The inertia of dipoles is size depended and is reflected by the occurring relaxation processes of different, although close, relaxation times. DRF expresses also the ability of the examined systems to store energy. At the maximum of the DRF curves the ability to store energy approaches 2.4 times that of the unreinforced epoxy.

3.3 Dynamic analysis of relaxation processes in SrTiO₃/epoxy nanocomposites

Relaxation processes occurring in polymers and polymer composite systems can be studied by different formalisms, such as dielectric permittivity, electric modulus, AC conductivity and complex impedance mode. All four formalisms are able to describe the electrical phenomena which appear in polymer composite systems. However, there are cases where one of them might be more suitable in studying the occurring physical mechanisms. In this work both imaginary part of dielectric permittivity and imaginary part of electric modulus were employed for describing the recorded relaxation processes. Electric modulus is defined as the inverse quantity of complex permittivity according to Eq. (5) [19]:

$$M^* = \frac{1}{\epsilon^*} = \frac{\epsilon'}{\epsilon'^2 + \epsilon''^2} + i \frac{\epsilon''}{\epsilon'^2 + \epsilon''^2} = M' + iM'' \quad (5)$$

where ϵ' , ϵ'' and M' , M'' are the real and imaginary part of dielectric permittivity and electric modulus respectively. Electric modulus is considered as an effective tool for the representation of dielectric data since it neglects electrode/specimen polarization and relevant capacitances [19, 20].

Figure 7a presents the frequency dependence of the imaginary part of electric modulus at 100 °C for all specimens, α -relaxation process is evident in all cases, through the formation of the loss peak. Loss peak position seems not to vary with filler content, which can be considered as indicative for good wetting and adhesion between matrix and nanoparticles. Specifically, in the case of fine dispersion of nanoparticles in the polymer matrix, an extensive surface area is formed, in which the polymer chains are in contact with nanoparticles. As the distribution of nanofiller improves, the extent of the interface increases. Depending on the roughness of the surface,

the existence of pores, the level of wetting of the nanofiller in the polymer matrix and the adhesion among them, the mobility of the macromolecules can be altered in comparison with the pure resin. In the case of poor wetting and poor adhesion, weak interactions between polymer chains and nanoinclusions occur, causing the shift of loss peak of the glass to rubber process to higher frequencies expressing the facilitation of the macromolecular relaxation and the resulting decrease of T_g [14, 16, 21].

Additionally, the slight decrease of loss peak maxima with filler content, denotes moderate to strong interactions between macromolecules and SrTiO₃ nanoparticles. Equation (5) denotes that a decrease of the imaginary part of electric modulus reflects an increase of dielectric loss, which actually implies the increase of the dissipated energy. It can be concluded that the interactions between the constituent phases exert moderate restrictions on the segmental relaxations of the polymer chains, which increase with the reinforcing phase content. On the other hand, Fig. 7b shows the variation of the imaginary part of dielectric permittivity upon temperature at 1 MHz, in this case, β -relaxation process appears via the formation of the loss peak. Evidently, dielectric loss increases with filler content, expressing the required enhanced energy by the polar side groups in order to follow the alternation of the applied field. Possibly the presence of nanoinclusions obstructs the orientation of side groups via spatial restrictions [18].

Relaxation dynamics can be studied by plotting the loss peak frequency as a function of reciprocal temperature for each system and for every relaxation process. The temperature dependence of the loss peak position of α -relaxation follows the Vogel–Fulcher–Tammann (VFT) equation which is expressed via Eq. (6):

$$f_{\max} = f_0 \exp \left[-\frac{B}{T - T_0} \right] \quad (6)$$

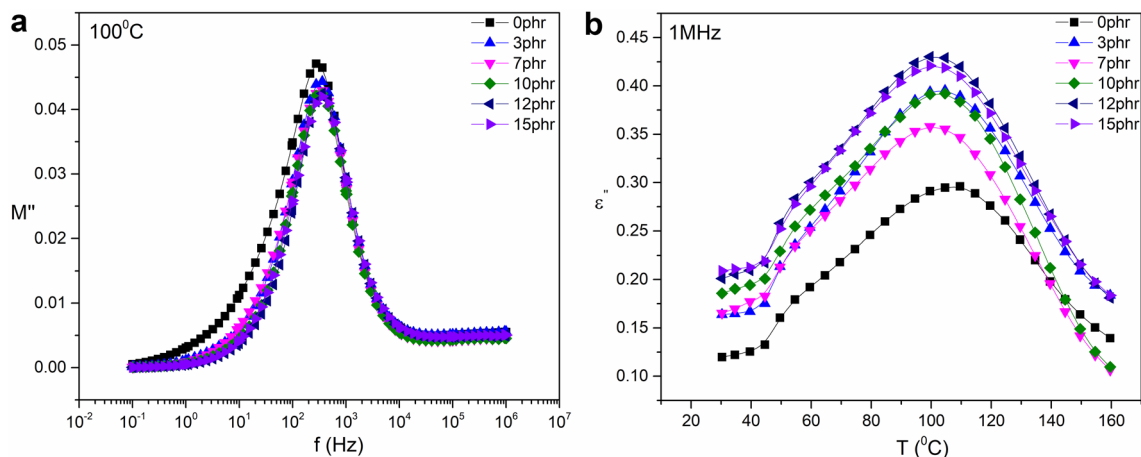


Fig. 7 **a** Imaginary part of electric modulus as a function of frequency at 100 °C and **b** imaginary part of dielectric permittivity as a function of temperature at 1 MHz

where f_0 is a pre-exponential factor, B is a parameter being the measure of the activation energy of the process, and T_0 the Vogel temperature or ideal glass transition, which has been found to lie between 30 and 70 K below the experimentally T_g value [20, 22]. The variation of loss peak position with temperature for β -relaxation and IP follows an Arrhenius type behaviour, which can be expressed via Eq. (7):

$$f_{\max} = f_0 \exp \left[-\frac{E_A}{kT} \right] \quad (7)$$

where f_0 is a pre-exponential factor, E_A is the activation energy of the corresponding mechanism and k is Boltzmann constant. The variation of loss peak frequency with temperature for α - and β -relaxation process is depicted in Fig. 8a, b. The limited loss peaks recorded in the case of IP-process lead to a fitting procedure of low reliability and thus it is not presented. Lines in Fig. 8a, b have been produced by fitting data with Eqs. 6 and 7 respectively. Obtained fitting parameters are listed in Table 1. Dynamics of α -relaxation process follows the VFT equation (Fig. 8a), since relaxation rate increases rapidly with decreasing temperature, due to the reduction of free volume. Glass to rubber transition is influenced by the presence of nanofiller inside the polymer matrix and more specific by the particle–particle and the polymer–particle interactions. Table 1 indicates that T_0 in nanocomposites slightly decreases, in general, compared with polymer matrix, indicating the absence of strong interactions between polymer chains and nanoinclusions and an insignificant decrease of T_g . The 10phr SrTiO₃ nanocomposite exhibits higher value of T_0 (approximately the same value with polymer matrix) and at higher filler content T_0 decreases acquiring the average value of nanocomposites. Furthermore, values of parameter B increase

Table 1 Activation energy and parameters extracted via fitting data with Eqs. 6 and 7 for all studied systems

Specimen's concentration (phr)	α -relaxation		β -relaxation E_A (eV)
	T_0 (K)	B (K)	
0	316.10	42.09	2.674
3	313.30	46.56	3.466
7	314.75	43.26	3.732
10	316.03	41.06	3.650
12	314.80	42.81	3.849
15	314.95	41.93	4.501

with filler content implying that the process is delayed, due to restrictions exerted by nanoparticles. At low filler content the nanoparticles are at a distance from each other and the macromolecules–nanoparticles interactions seem to dominate. The reduction of parameter B observed for the 7 phr SrTiO₃ nanocomposite indicates a facilitation of the α -process, which can be attributed to the strengthening of the particle–particle interactions. These interactions are strengthening due to the increased content of nanoinclusions, which result in shorter distances between of them. At higher filler content, parameter B decreases further implying that the particle–particle interactions are the dominating ones [20, 23].

Figure 8b presents the variation of the loss peak position of β -relaxation process with the reciprocal temperature. Dielectric data can be described via the Arrhenius equation. Determined values of activation energy are listed in Table 1. Activation energy increases, steadily, with filler content reaching the highest value for the 15 phr SrTiO₃ nanocomposite. This finding is in accordance with Fig. 7b and confirms that the presence of nanoinclusions obstructs

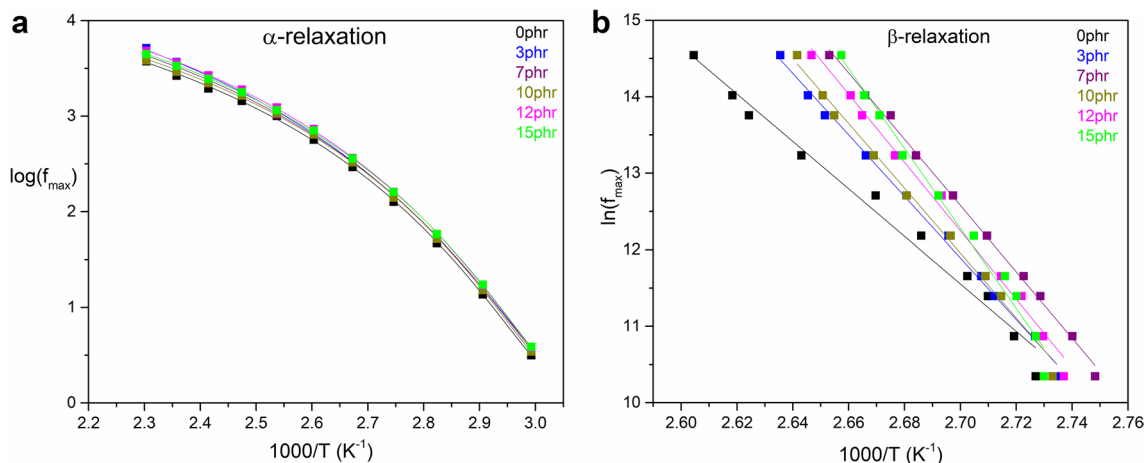


Fig. 8 Loss peak position as a function of the reciprocal temperature for all examined SrTiO₃/epoxy nanocomposites for the α -relaxation and β -relaxation process. Solid lines represent fittings of data via Eqs. 6 and 7 respectively

the orientation of polar side groups, due to spatial restrictions and possibly because of the mutual interactions between nanoparticles and the formation of small clusters at the higher filler loading.

4 Conclusion

SrTiO₃/epoxy nanocomposites were fabricated and studied varying the filler content of the reinforcing phase. Morphological and structural characterization was performed in all nanocomposite systems via XRD and SEM and it was verified that all specimens were successfully fabricated. Dielectric spectra reveal three relaxation processes: (a) glass to rubber transition of the polymer matrix (α -mode), (b) rearrangement of the polar side groups of the main polymer chain (β -mode) and (c) interfacial polarization (IP effect) arising from the electrical heterogeneity of the systems. Dielectric Reinforcing Function (DRF) was employed in order to investigate the functional behaviour and the energy storing efficiency of all examined specimens. Finally, relaxation dynamics of the α -relaxation and β -relaxation was studied.

References

1. T. Hanneman, D.V. Szabo, *Materials* **3**, 3468 (2010)
2. P. Barber, S. Balasubramanian, Y. Anguchamy, S. Gong, A. Wibowo, H. Gao, H.J. Ploehn, H.-C. Zur Loye, *Materials* **2**, 1697 (2009)
3. L.B. Kong, S. Li, T.S. Zhang, J.W. Zhai, F.Y.C. Boey, J. Ma, *Prog. Mater. Sci.* **55**, 840 (2010)
4. Z.-M. Dang, J.-K. Yuan, J.-W. Zha, T. Zhou, S.-T. Li, G.-H. Hu, *Prog. Mater. Sci.* **57**, 660 (2010)
5. D. Tan, P. Irwin, In *Polymer Baser Nanodielectric Composite*, In: C. Sikalidis, (ed) (In Tech, 2011), p. 115
6. M.F. Frechette, M.L. Trudeau, H.D. Alamdari, S. Boily, *IEEE Trans. Dielect. Electr. Insul.* **11**, 808 (2004)
7. Prateek, V.K. Thakur, R.K. Gupta, *Chem. Rev.* **116**, 4260 (2015)
8. E. Baer, L. Zhu, *Macromolecules* **50**, 2239 (2017)
9. T. Tanaka, T. Imai, *Advanced Nanodielectric Fundamentals and Applications* (Taylor and Francis, Pan Stanford Publishing, Abingdon, 2017)
10. T. Tanaka, *IEEE Trans. Dielect. Electr. Insul.* **12**, 237 (2005)
11. Y.-P. Cai, D.-Z. Han, R.Y. Ning, *Chin. J. Chem. Phys.* **23**, 237 (2010)
12. R.A. Cowley, *Philos. Trans. R. Soc. A* **354**, 2799 (1996)
13. S. Singha, M.J. Thomas, *IEEE Trans. Dielect. Electr. Insul.* **15**, 12 (2008)
14. G.C. Psarras, in *Conductivity and Dielectric Characterization of Polymer Nanocomposites*, ed. by S.C. Tjong, Y.W. Mai (Woodhead Publishing Limited, Cambridge, 2010), p. 31
15. A.K. Jonscher, *Universal Relaxation law* (Chelsea Dielectric Press, London, 1992)
16. G.C. Psarras, in *Fundamentals of dielectric theories*, ed. by Z.M. Dang (Elsevier Inc, Cambridge, 2018), p. 11
17. G. Ioannou, A. Patsidis, G.C. Psarras, *Compos. A* **42**, 104 (2011)
18. A.C. Patsidis, K. Kalaitzidou, G.C. Psarras, *Mater. Chem. Phys.* **135**, 798 (2012)
19. G.M. Tsangaris, G.C. Psarras, N. Kouloumbi, *J. Mater. Sci.* **33**, 2027 (1998)
20. A. Patsidis, G.C. Psarras, *Express Polym. Lett.* **2**, 718 (2008)
21. H. Lu, S. Nutt, *Macromolecules* **36**, 4010 (2003)
22. O. Vryonis, D.L. Anastassopoulos, A.A. Vardis, G.C. Psarras, *Polymer* **95**, 82 (2016)
23. P.K. Karahaliou, A.P. Kerasidou, S.N. Georga, G.C. Psarras, C.A. Krontiras, J. Karger-Kocsis, *Polymer* **55**, 6819 (2014)

Publisher's Note Springer Nature remains neutral with regard to jurisdictional claims in published maps and institutional affiliations.